*J. Fluid Mech.* (1967), *vol.* 28, *part* 2, *pp.* 323–336
*Printed in Great Britain*



# A numerical study of the time-dependent viscous flow between two rotating spheres

By CARL E. PEARSON
The Boeing Company, Renton, Washington†

(Received 18 July 1966)

An extension of numerical methods described in previous papers is used to analyse the time-dependent rotationally-symmetric motion of an incompressible viscous fluid contained between two concentric spheres having a common axis of rotation. The motion is governed by a pair of coupled non-linear partial differential equations in three independent variables, with singular end conditions. The computational process is described, and numerical solutions are presented for cases in which one (or both) of the spheres is given an impulsive change in angular velocity—starting from a state of either rest or uniform rotation. Reynolds numbers lie in the range 10–1500.

## 1. Introduction

The motion of a viscous fluid in a rotating container is of interest in engineering design (centrifuges, fluid gyroscopes) and also in geophysics. We consider here a spherical geometry, in which an incompressible viscous fluid is contained between two concentric spheres whose angular velocities about a common axis of rotation may be arbitrarily-prescribed functions of time. We restrict our attention to rotationally-symmetric motions. Such motions may be described in terms of a pair of coupled non-linear partial differential equations in three independent variables; one is of second order, and the other is of fourth order. The differential operators involved in these equations become singular at the polar boundaries.

Available theoretical work concerning such problems is primarily of a boundary-layer or singular-perturbation character; we mention Howarth (1951), Proudman (1956), Lord & Bowden (1963), Fox (1964), Greenspan (1964) and Carrier (1966). Our purpose is to examine the way in which numerical methods can supplement or extend such analytical studies.

As might be expected, there are problems of accuracy, stability, and excessive computer time encountered in developing numerical solutions for problems of this kind. It is important to provide means for reliable verification of computer solutions. Our computational procedure is an extension of the methods previously used for an injection problem and for a rotating disk problem (Pearson 1965*a*, *b*). It is described in detail in § 3. Verification methods are discussed in § 4; one ingredient in this verification is an apparently new exact analytical solution of the Navier–Stokes equations.

† The first part of this work was carried out at the Sperry Rand Research Center in Sudbury, Mass.

§5 gives computational results for a selection of problems which includes:

(*a*) steady-state flow patterns for rotation of outer sphere alone, for Reynolds numbers of 10, 100, 1000;

(*b*) time-dependent flow patterns for case in which one of the spheres is started from rest;

(*c*) spin-up problem, in which mutual angular velocities of both spheres are altered by small amount (or by large amount) from initial state of uniform rotation;

(*d*) case in which angular velocity of inner sphere is suddenly reduced, starting from state of uniform rotation.

In all of these cases, the inner radius was one-half the outer. The Reynolds number was usually chosen in the range 1000–1500. The number of mesh points used ranged from 800 to 3200; about one to six hours of 7094 Mod II time was required per problem.

## 2. Equations of motion

Consider the region between two concentric spheres, as shown in figure 1. Each sphere may rotate independently about the $Z$-axis. Only rotationally symmetric motions are considered, so that all quantities are independent of the azimuthal angle. The velocity components in the directions of increasing $r$ and $\theta$ are $u$ and $v$, respectively; the velocity perpendicular to the meridional plane is $w$. For incompressible flow, the Navier–Stokes equation implies (Rosenhead 1963)

$$u = \psi_\theta / r^2 \sin\theta,$$

$$v = -\psi_r / r \sin\theta,$$

$$w = \Omega / r \sin\theta,$$

$$(\partial\Omega/\partial t) - \frac{\psi_r \Omega_\theta - \psi_\theta \Omega_r}{r^2 \sin\theta} = \nu D^2 \Omega, \tag{1}$$

$$\frac{\partial}{\partial t}(D^2\psi) + \frac{2\Omega}{r^3 \sin^2\theta}[\Omega_r r\cos\theta - \Omega_\theta \sin\theta]$$

$$- \frac{1}{r^2 \sin\theta}[\psi_r (D^2\psi)_\theta - \psi_\theta (D^2\psi)_r]$$

$$+ \frac{2D^2\psi}{r^3 \sin^2\theta}[\psi_r r\cos\theta - \psi_\theta \sin\theta] = \nu D^4 \psi, \tag{2}$$

where

$$D^2 = \frac{\partial^2}{\partial r^2} + \frac{1}{r^2}\frac{\partial^2}{\partial\theta^2} - \frac{1}{r^2}\cot\theta\frac{\partial}{\partial\theta}, \tag{3}$$

where $\psi$ is the stream function, $\nu$ the kinematic viscosity, and where subscripts denote partial derivatives.

Let $R_0$ and $\omega_0$ be reference values of radius and angular velocity, respectively. Then non-dimensional quantities (denoted by asterisks) can be defined via

$$r = r^* R_0, \quad u = u^* R_0 \omega_0, \quad \psi = \psi^* R_0^3 \omega_0,$$

$$t = t^*/\omega_0, \quad \Omega = \Omega^* R_0^2 \omega_0.$$

With these substitutions, (1) and (2) retain their form, except that all quantities are replaced by their dimensionless equivalents, and $\nu$ is replaced by $1/Re$, where the Reynolds number $Re$ is defined by

$$Re = \omega_0^2 R_0/\nu. \tag{4}$$

We consider that this change has been made, so that (1) and (2) are now non-dimensional; $\nu$ is considered replaced by $1/Re$, and we drop the asterisks. We choose $R_0$ = radius of outer sphere.

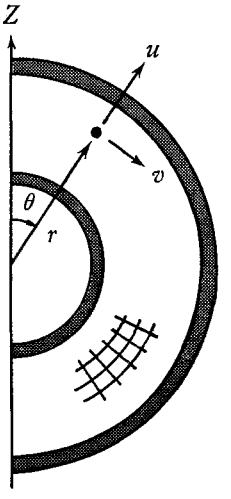


FIGURE 1. Region between two spheres.

The boundary conditions are clearly that $\psi = \partial\psi/\partial n = 0$ on the boundaries of the region of figure 1, and that $\Omega$ is prescribed on all of these boundaries (note that $\Omega = 0$ at $\theta = 0, \pi$). Moreover,

$$\begin{aligned} D^2\psi &= (u_\theta - rv_r - v)\sin\theta \\ &= 0 \quad \text{at} \quad \theta = 0, \pi. \end{aligned} \tag{5}$$

Some of the coefficients in (1) and (2) are singular at $\theta = 0, \pi$; this implies that the quantities multiplied by these coefficients must vanish at $\theta = 0, \pi$. Contrary to initial expectation, these coefficient singularities did not result in any computational difficulties, and this is perhaps reasonable, for the boundaries at $\theta = 0, \pi$ are lines rather than surfaces and so have only a relatively weak influence on the nature of the solution of a problem in three space dimensions (rotational symmetry does not affect this basic characteristic).

## 3. Computational procedure

We will describe here only the general outline of the computational procedure; further details will be found elsewhere (Pearson 1966).

The region of figure 1 is covered by a mesh, as indicated in the lower portion of that figure. Let $\Delta\theta$ and $\Delta r$ denote the mesh spacing in the directions of increasing

$\theta$ and $r$ respectively, and let $\Delta t$ denote the increment in time. Let $\phi_{ij}^n$ denote the value of any quantity $\phi$ at time $n\Delta t$ and at position $\theta = i\Delta\theta$, $r = R_I + j\Delta r$, where $R_I$ is the inner radius. The computational process consists in using previously determined values of $\psi$, $D^2\psi$, and $\Omega$ at times $n\Delta t$, $(n-1)\Delta t$, and $(n-2)\Delta t$, together with numerical approximations to (1) and (2), to determine values of these quantities at times $(n+1)\Delta t$. The procedure is as follows.

(i) Extrapolate parabolically to obtain *approximate* values of $\psi$ and $D^2\psi$ at all mesh points, at time $(n+1)\Delta t$. (In particular, $\psi^{n+1} = 0$ on all boundary mesh points.)

(ii) Insert values for $\Omega^{n+1}$ at all boundary mesh points, as prescribed by given angular velocity histories of spheres.

(iii) Use (1) to determine approximate values for $\Omega^{n+1}$ at all interior mesh points; this is done in two half-steps, using the implicit alternating direction method (for reasons of stability and accuracy) described in note 1 below. The procedure makes use of the current approximations to the $\psi^{n+1}$ values.

(iv) Use (2) to determine approximate values for $(D^2\psi)^{n+1}$ at all interior mesh points, using the current approximations to $\Omega^{n+1}$, $\psi^{n+1}$, and boundary values of $(D^2\psi)^{n+1}$. Again this is done in two half-steps, of the character discussed in note 1.

(v) Using the values of $(D^2\psi)^{n+1}$ determined in step (iv), and the prescribed values of $\psi^{n+1}$ on the boundary, use successive over-relaxation to solve the equation

$$D^2\psi = \psi_{rr} + r^{-2}\psi_{\theta\theta} - r^{-2}\cot\theta\,\psi_\theta$$

for values of $\psi^{n+1}$ at interior mesh points.

(vi) Although the values of $\psi^{n+1}$ obtained in step (v) provide improvements over previous approximations, the direct replacement of the previous values by these new values is found to lead to overall computational instability. Consequently, a weighting procedure is used, in which previous values $(\psi^{n+1})_{\text{old}}$ are replaced by new values $(\psi^{n+1})_{\text{new}}$ via the formula

$$(\psi^{n+1})_{\text{new}} = S(\psi^{n+1})_{\text{old}} + (1-S)(\psi^{n+1})_5, \tag{6}$$

where $(\psi^{n+1})_5$ denotes the values obtained in step (v). The optimal value of the weighting factor $S$ depends somewhat on Reynolds number, but is typically about 0·7.

(vii) Use the boundary condition $\partial\psi/\partial n = 0$, together with the $\psi^{n+1}$ values near the boundary as found in step (vi), in Taylor series expansions so as to obtain improved values of $(D^2\psi)^{n+1}$ on boundary mesh points. (The use of several terms of the Taylor series expansion is essential for accuracy in high-order equation systems.) Again, a weighted combination of the 'new' and 'old' values for $(D^2\psi)^{n+1}$ must be formed; the weighting factor $S$ in the equation analogous to (6) is typically 0·92.

(viii) Return to step (iii), and continue iteration through these computational steps until a convergence criterion is satisfied. The time step is then complete.

### *Note* 1

The first half time step for (1) is given here as typical of the implicit alternating direction procedure used in steps (iii) and (iv). Notice that values of $\Omega^{n+\frac{1}{2}}$, the

unknown, are used in all differences involving the subscript $i$; in the second half step, the unknown values of $\Omega^{n+1}$ would appear in all differences involving the subscript $j$. The sets of implicit equations that result are easily solved by Gaussian elimination. This procedure is an extension to non-linear equations of the method used by Peaceman & Rachford (1955) for diffusion equation problems; it can be shown to possess substantial advantages of accuracy and computational stability over such explicit methods as those of DuFort & Frankel (1953).

$$\Omega_{ij}^{n+\frac{1}{2}}\left\{1+\frac{\Delta t}{r_j^2(\Delta\theta)^2 Re}\right\} = \Omega_{i+1,j}^{n+\frac{1}{2}}\left\{\frac{\Delta t}{2Re.r_j^2.(\Delta\theta)^2}-\frac{\Delta t\cot\theta_i}{4Re r_j^2.\Delta\theta}\right.$$

$$\left.+\frac{\Delta t}{8r_j^2\sin\theta_i\Delta r\Delta\theta}[\tfrac{3}{4}(\psi_{i,j+1}^n-\psi_{i,j-1}^n)+\tfrac{1}{4}(\psi_{i,j+1}^{n+1}-\psi_{i,j-1}^{n+1})]\right\}$$

$$+\Omega_{i-1,j}^{n+\frac{1}{2}}\left\{\frac{\Delta t}{2Re.r_j^2(\Delta\theta)^2}+\frac{\Delta t\cot\theta_i}{4Re.r_j^2.\Delta\theta}\right.$$

$$\left.-\frac{\Delta t}{8r_j^2\sin\theta_i\Delta r\Delta\theta}[\tfrac{3}{4}(\psi_{i,j+1}^n-\psi_{i,j-1}^n)+\tfrac{1}{4}(\psi_{i,j+1}^{n+1}-\psi_{i,j-1}^{n+1})]\right\}$$

$$+\frac{\Delta t}{2Re.(\Delta r)^2}\{\Omega_{i,j+1}^n+\Omega_{i,j-1}^n-2\Omega_{i,j}^n\}$$

$$+\Omega_{i,j}^n-\frac{\Delta t}{8r_j^2\sin\theta_i\Delta r\Delta\theta}\{\Omega_{i,j+1}^n-\Omega_{i,j-1}^n\}\{\tfrac{3}{4}(\psi_{i+1,j}^n-\psi_{i-1,j}^n)+\tfrac{1}{4}(\psi_{i+1,j}^{n+1}-\psi_{i-1,j}^{n+1})\}.$$

*Note 2*

The results of § 5 correspond to situations in which the angular velocity of one or both of the spheres is impulsively changed. Computationally, this necessitated a special treatment, in that the first time step was replaced by a large number of smaller time steps; that this process is appropriate is shown in Pearson (1965*c*).

## 4. Verification of computer solutions

In addition to the requirement that the flow fields on the two sides of the equator be symmetrical, and that decreases in the space and time mesh intervals should produce no significant change in the calculated results, the computer solutions were verified in the following ways.

### (*a*) *Low Re number solutions in steady state*

If the non-linear terms in (1) and (2) are negligible, then we can set $\Omega = f(r)\sin^2\theta$ for the steady-state solution to yield $f''-(2/r^2)f=0$. With outer radius $= R_0 = 1$, and inner radius $= \frac{1}{2}$, consider the case in which the outer sphere is given unit angular velocity (relative to the reference values $\omega_0$) and in which the inner sphere is held at rest. Then (11) requires that

$$f = \tfrac{8}{7}r^2-\tfrac{1}{7}r^{-1}.$$

In (2), the first non-linear term on the left-hand side provides the 'driving force' for this equation and so cannot be neglected. The substitution $\Omega = f(r)\sin^2\theta$ suggests that $\psi$ should have the form $g(r)\sin^2\theta\cos\theta$, and we find

$$\psi = (10^{-3}Re)(1-r)^2(r-\tfrac{1}{2})^2[8{\cdot}69r + 26{\cdot}07 + 9{\cdot}73r^{-1} - 1{\cdot}78r^{-2}]\sin^2\theta\cos\theta. \quad (7)$$

For the choice $Re = 10$ (cf. figure 2), these formulas gave results agreeing to within 4 or 5 significant figures with the results obtained by the computational procedure of § 3 (using a $40 \times 20$ mesh).

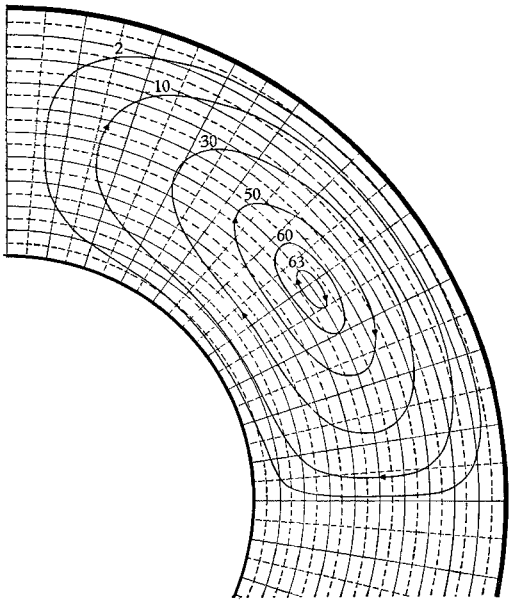


FIGURE 2. Contour lines of $10^5\psi$ for $Re = 10$, $T = 7{\cdot}05$. Inner sphere held fixed, outer started at $T = 0$ with $\omega = 1$. (Note: flow is very close to this even at $T = 1$).

### (*b*) *Short time solution*

Even for large values of $Re$, the non-linear terms in (1) and (2) are small, for small $t$, for situations in which one or both spheres are started from rest, and all except the first such term on the left-hand side of (2) may be neglected. We write $\Omega = f(r,t)\sin^2\theta$, and find

$$f_t = (f_{rr} - 2f/r^2)/Re. \quad (8)$$

For the case in which the outer sphere is impulsively given unit angular velocity, (8) may be solved by Laplace transforms; the solution behaviour can be determined for short values of $t$ by considering large values of the transform variable, and this leads to the asymptotic result

$$f \sim \operatorname{erfc}[(1-r)(Re)^{\frac{1}{2}}/2t^{\frac{1}{2}}] - \operatorname{erfc} r(Re)^{\frac{1}{2}}/2t^{\frac{1}{2}}.$$

For values of $Re = 10$, 100, 1000, this formula gave results in excellent agreement with those obtained by the procedure of § 3, for small values of $t$.

### (*c*) *Ring vortex problem*

The functions

$$\psi = \exp\{-\alpha^2(t/Re)\}\sqrt{r}J_{\pm(n+\frac{1}{2})}(\alpha r).\sin^2\theta.P_n'(\cos\theta), \quad \Omega = \alpha\psi, \quad (9)$$

provide an exact (and apparently new) solution of (1) and (2); the corresponding fluid motion is that of a set of oppositely-rotating ring vortices. The boundary conditions on the spherical surfaces that correspond to this solution were imposed,

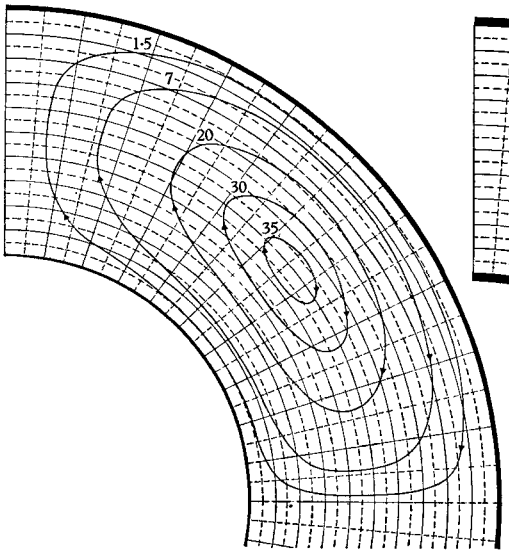


FIGURE 3

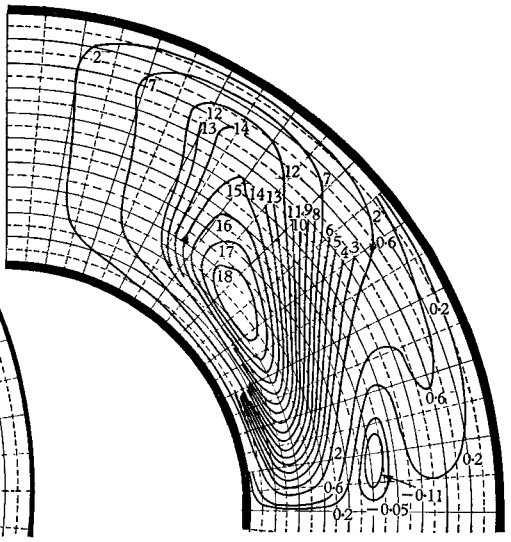


FIGURE 4

FIGURE 3. Contour lines of $10^4\psi$ for $Re = 100$, $T = 62$ (essentially steady state). Inner sphere held fixed, outer started impulsively with $\omega = 1$.

FIGURE 4. Contour lines of $10^4\psi$ for $Re = 1000$, $T = 223$. Inner sphere held fixed, outer started impulsively with $\omega = 1$.

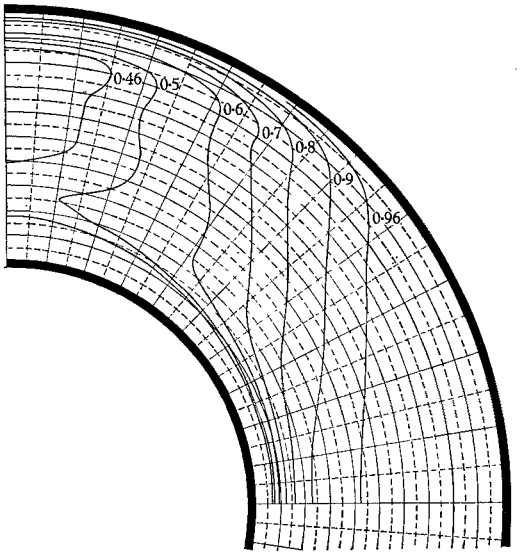


FIGURE 5. Contour lines of angular velocity for $Re = 1000$, $T = 223$. Outer sphere started impulsively at $T = 0$.

and the procedure of § 3 was used to follow the motion computationally; the computed results were found to be in close agreement with those given by the above exact solution.

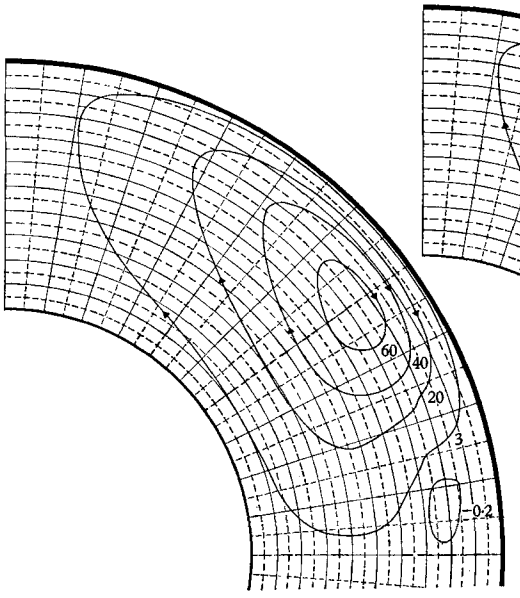


FIGURE 6

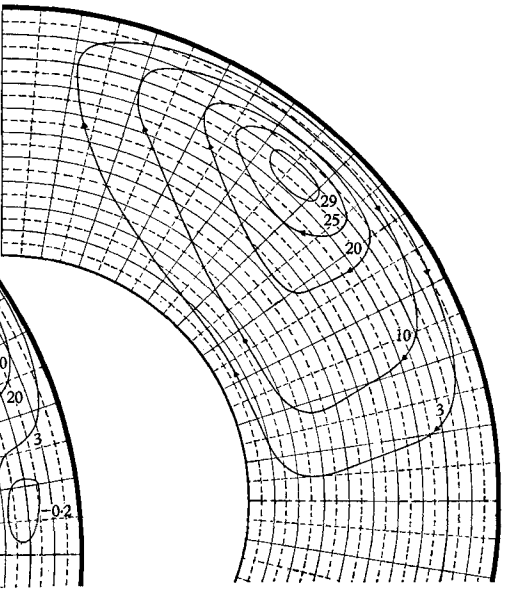


FIGURE 7

FIGURE 6. Contour lines of $10^4\psi$ for $Re = 1000$, $T = 8$. Inner sphere held fixed, outer started impulsively with $\omega = 1$.

FIGURE 7. Contour lines of $10^4\psi$ for $Re = 1000$, $T = 18$. Inner sphere held fixed, outer started impulsively with $\omega = 1$.

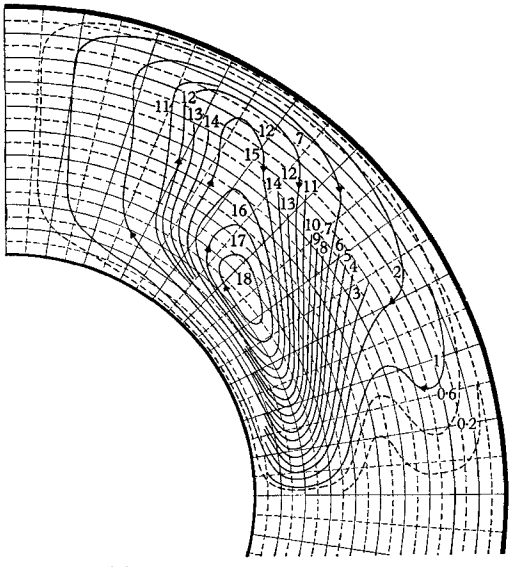


FIGURE 8. Contour lines of $10^4\psi$ for $Re = 1000$, $T = 47$. Inner sphere held fixed, outer sphere started impulsively at $T = 0$.

## 5. Computed fluid motions

In all cases, the radius of the inner sphere was taken as $\frac{1}{2}$ that of the outer sphere.

Figures 2, 3 and 4 show the steady-state flow patterns (contour lines of stream function $\psi$) for the case in which the inner sphere is held fixed and the outer given

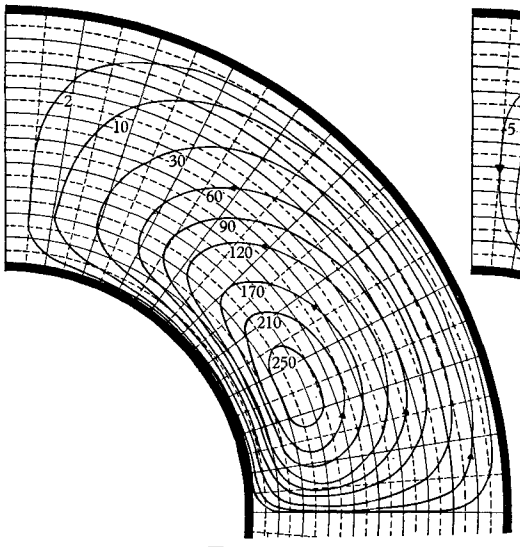


FIGURE 9

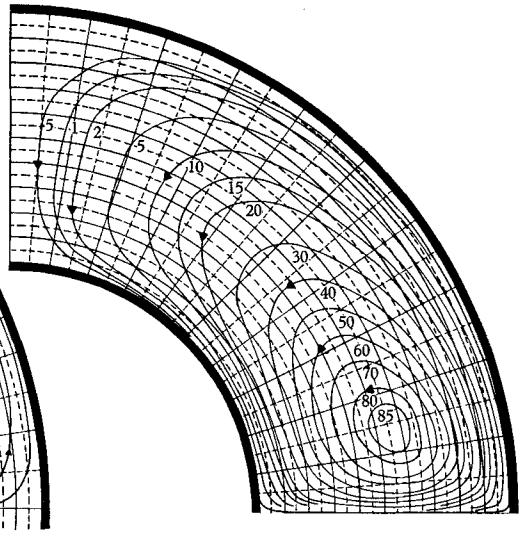


FIGURE 10

FIGURE 9. Contour lines of $-\psi \times 10^5$ for $Re = 1000$, $T = 5$. Outer sphere held fixed, inner started impulsively at at $T = 0$ with $\omega = 1$.

FIGURE 10. Contour lines of $-\psi \times 10^4$ for $Re = 1000$, $T = 443$. Outer sphere held fixed, inner started impulsively at $T = 0$ with $\omega = 1$.

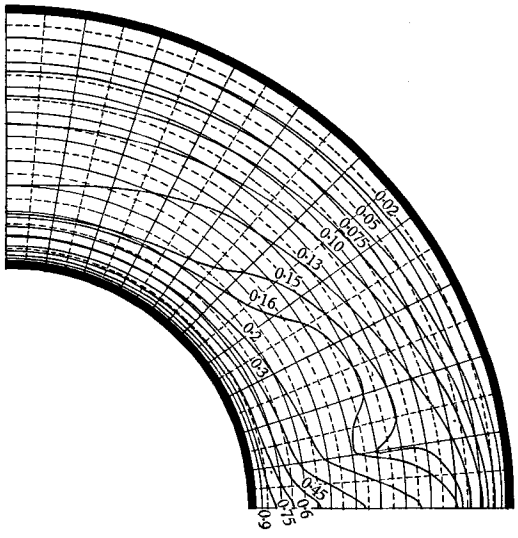


FIGURE 11. Contour lines of angular velocity for $Re = 1000$, $T = 443$. Outer sphere held fixed, inner started impulsively at $T = 0$ with $\omega = 1$.

unit angular velocity, for Reynolds numbers of 10, 100, and 1000 respectively. For $Re = 10$, the flow patterns agreed very closely with those described by (7); for $Re = 100$, the non-linear terms were sufficiently important that (7) gave results in error by a factor of 2. Figure 4 shows that at $Re = 1000$ most of the circulation tends to lie in a cylindrical sheath of radius approximately equal to

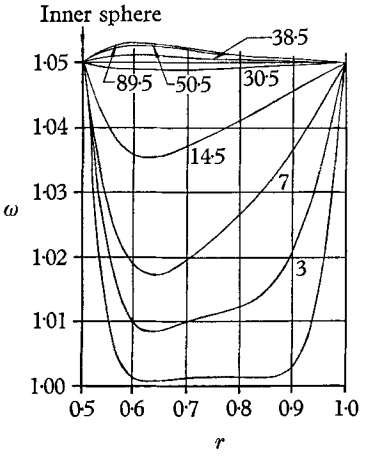


FIGURE 12. Angular velocity profile at $\theta = 90°$ for spin-up case $Re = 1000$.

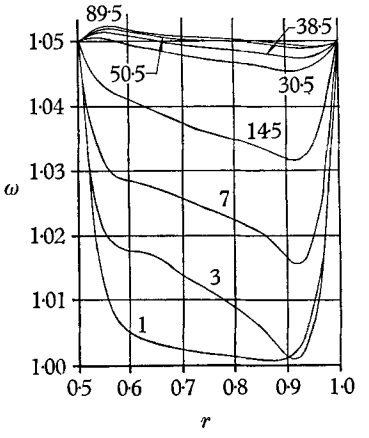


FIGURE 13. Angular velocity profile at $\theta = 45°$ for spin-up case $Re = 1000$.

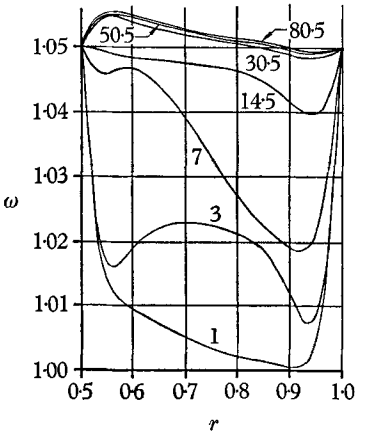


FIGURE 14. Angular velocity profile at $\theta = 4\frac{1}{2}°$ for spin-up case $Re = 1000$.

that of the inner sphere; also, there is a recirculation zone near the equator. The angular velocity profiles for this $Re = 1000$ case are shown in figure 5, and it is seen that, outside the cylindrical sheath region, the rotation is almost of solid body character.

For $Re = 1000$, several stages in the build up of the steady-state motion of figure 4 are shown in figures 6, 7 and 8. At $T = 8$, a recirculation zone appeared, and persisted until about $T = 12$; by $T = 47$, the flow had begun to acquire its cylindrical sheath character, but the steady-state recirculation zone had not yet reappeared.

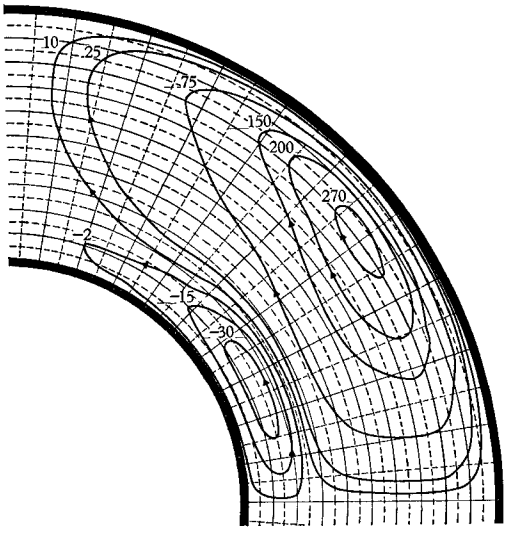


FIGURE 15. Contour lines for $10^6\psi$. Inner and outer spheres spun-up together from $\omega = 1$ to $\omega = 1{\cdot}05$. $Re = 1000$, $T = 7$.

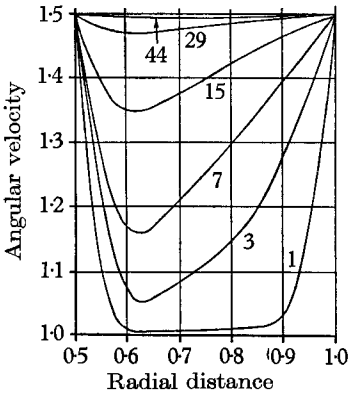


FIGURE 16. Angular velocity profile at $\theta = 90°$. Spin-up from $\omega = 1{\cdot}0$ to $\omega = 1{\cdot}5$.

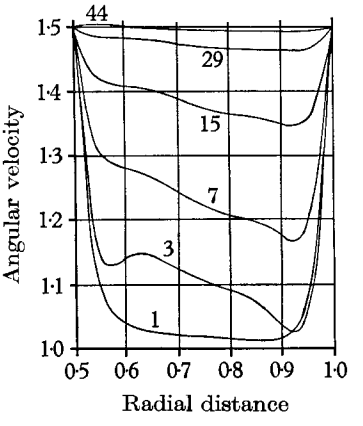


FIGURE 17. Angular velocity profile at $\theta = 45°$. Spin-up from $\omega = 1{\cdot}0$ to $\omega = 1{\cdot}5$.

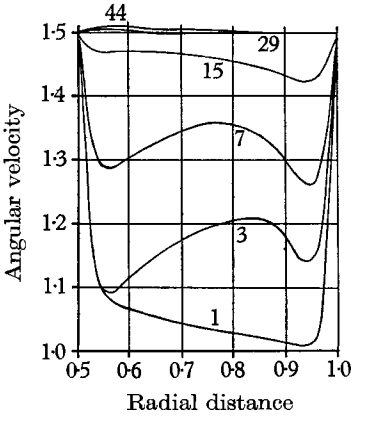


FIGURE 18. Angular velocity profile at $\theta = 4\frac{1}{2}°$. Spin-up from $\omega = 1{\cdot}0$ to $\omega = 1{\cdot}5$.

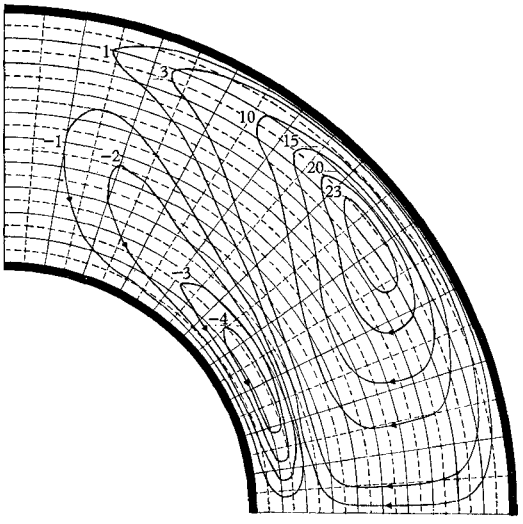


FIGURE 19. Contour lines for $10^4\psi$. Two spheres spun-up together from $\omega = 1$ to $\omega = 1{\cdot}5$. $Re = 1000$, $T = 7$.

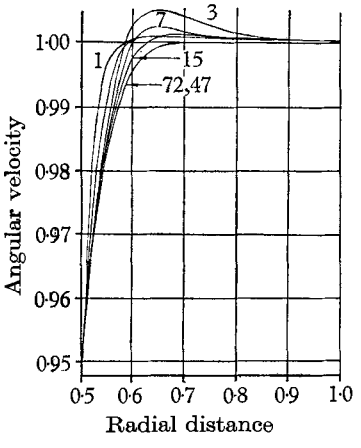


FIGURE 20. $\theta = 90°$. Inner sphere slowed to $\omega = 0{\cdot}95$.

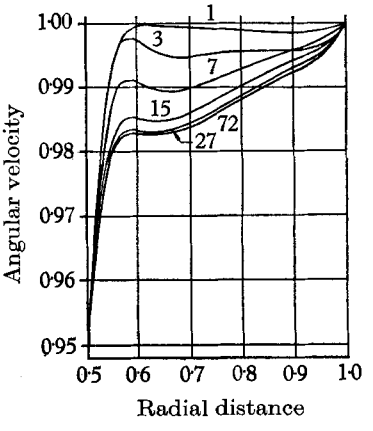


FIGURE 21. $\theta = 45°$. Inner sphere slowed to $\omega = 0{\cdot}95$.

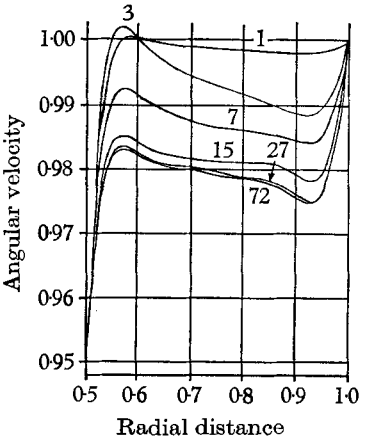


FIGURE 22. $\theta = 4\frac{1}{2}°$. Inner sphere slowed to $\omega = 0{\cdot}95$.

Figures 9 and 10 depict the contour lines of $\psi$, at times $T = 5$ and $T = 443$, respectively, for the case in which the outer sphere is held fixed and the inner given unit angular velocity at $T = 0$. Note the relatively sharp flow concentration in the equatorial region. Angular velocity profiles are shown in figure 11.

The next sequence of figures relate to the 'spin-up' problem, in which, starting from a steady-state angular velocity of unity (solid body rotation with $Re = 1000$) both spheres are given the same impulsive increase in angular velocity. For the

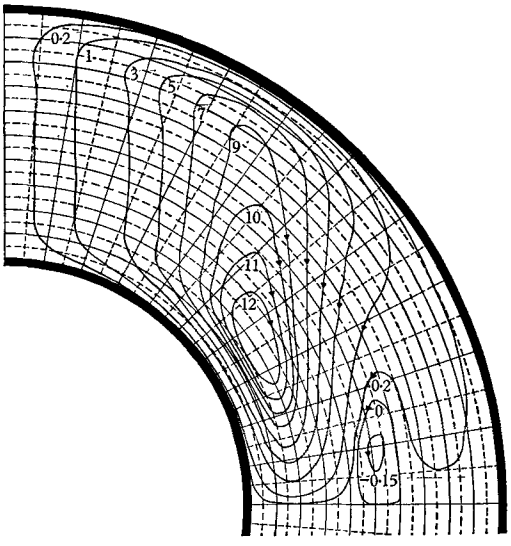


FIGURE 23. Contour lines of $10^5\psi$. For case in which angular velocity of inner sphere is impulsively reduced to 0·95; that of outer sphere remains unaltered at 1·0. $Re = 1000$, $T = 72$ (essentially steady-state).

case in which this increase is from $\omega = 1$ to $\omega = 1{\cdot}05$ (small perturbation), profiles of angular velocity at various times are given in figures 12, 13 and 14, corresponding to $\theta = 90°$, 45° and $4\frac{1}{2}°$, respectively. Note the overshoot near the inner sphere. Contour lines of $\psi$ at an early stage of the motion ($T = 7$) are shown in figure 15. Corresponding results for the case in which the spin-up is from $\omega = 1$ to $\omega = 1{\cdot}5$ (large perturbation) are shown in figures 16, 17, 18 and 19.

The final case studied was that in which, starting from solid-body type rotation at $\omega = 1$, $Re = 1000$, the angular velocity of the inner sphere alone was impulsively altered to $\omega = 0{\cdot}95$ at $T = 0$. Angular velocity profiles at $\theta = 90°$, 45° and $4\frac{1}{2}°$ are shown for various times in figures 20, 21 and 22; the resulting steady-state stream function contour lines are shown in figure 23. A weak recirculation zone is in evidence.

## REFERENCES

CARRIER, G. F. 1966 *J. Fluid Mech.* **24**, 641.

DU FORT, E. C. & FRANKEL, S. P. 1953 *M.T.A.C.* **7**, 135.

FOX, J. 1964 *NASA TN* D-2491.

GREENSPAN, H. P. 1964 *J. Fluid Mech.* **21**, 673.

HOWARTH, L. 1951 *Phil. Mag. Ser.* 7, **42**, 1308.

LORD, R. G. & BOWDEN, F. P. 1963 *Proc. Roy. Soc.* A **271**, 143.
PEACEMAN, D. W. & RACHFORD, H. H. 1955 *J. Soc. Ind. App. Math.* **3**, 28.
PEARSON, C. E. 1965*a* *J. Fluid Mech.* **21**, 611.
PEARSON, C. E. 1965*b* *J. Fluid Mech.* **21**, 623.
PEARSON, C. E. 1965*c* *Math. of Computation*, **19**, 570.
PEARSON, C. E. 1966 *Proc. SIAM Symp. Num. Anal.* (to appear).
PROUDMAN, I. 1956 *J. Fluid Mech.* **1**, 505.
ROSENHEAD, L. 1963 *Laminar Boundary Layers.* Oxford University Press.